Trajectory Tracking in the Sagittal Plane: Decoupled Lift/Thrust Control via Tunable Impedance Approach in Flapping-Wing MAVs

Hosein Mahjoubi, and Katie Byl

Abstract—**Flapping-wing micro-aerial vehicles (MAVs) are a relatively new field of research in the robotics community. Inspired by insects, their small size and unique means of force production present many challenges, from morphological construction and power supply to control methodology. Over the past couple of decades, investigating the aeromechanics of insect flight and development of prototypes have been a major focus of most researchers in this field. Those works concentrating on force manipulation and motion control often rely on modifying the properties of wing-beat profile. However, such changes affect both lift and thrust simultaneously, making it very difficult to control these forces independently. The tunable impedance (TI) approach is an alternate method of force manipulation that modifies mechanical impedance properties of the wings rather than their stroke characteristics. In this work, we show how TI can be used to achieve decoupled lift/thrust control. A motion controller developed based on this feature enables a fly-sized model to track given trajectories in the sagittal plane. Results of simulated experiments with various types of trajectories demonstrate a high degree of precision and maneuverability.**

Keywords—Tunable Impedance; Micro-Aerial Robotics; Trajectory Tracking; Lift/Thrust Control; Insect Flight; Maneuverability; Simulation.

I. Introduction

Over recent decades, progress in miniaturization, from sensor, actuator and microprocessor design to micro-fabrication methods and low-power technologies, has turned the development of micro-aerial vehicles (MAVs) into a real possibility. These vehicles have the potential to revolutionize observation and information gathering operations and may be employed in a wide range of applications including environmental monitoring and homeland security. As a result, a growing number of researchers are now focusing on flight analysis, design and control of such systems.

Design solutions are often inspired by research on insect flight and the involved aerodynamics [1]-[6]. The main focus of recent research on flapping-wing MAVs is development of flapping mechanisms that are capable of producing sufficient lift for levitation. Several prototypes capable of takeoff and vertical flight have been developed over the past few years [7]-[9]. With such platforms available, force manipulation and motion control are the next challenges that must be faced. Recent work focused on vertical acceleration and altitude control has led to some impressive results [10]-[11]. Research on forward flight control has been less developed in comparison [12].

The majority of works concentrating on force control employ modifications in wing-beat profile to achieve their objective [13]-[14]. While this approach proves to be successful in separate control of lift [15] or horizontal thrust [16], simultaneous control of these forces is more challenging. Both forces are directly influenced by velocity of air flow over the wings, a factor that is heavily determined by the rate of wing-beat [17]. Therefore, modifying wing-beat profile will lead to a coupling between lift and thrust forces, i.e. an inconvenience for motion control and maneuverability of the vehicle.

Passive pitch rotation of the wing [18] is another phenomenon that plays a significant role in production and manipulation of lift/thrust through adjusting the angle of attack (AoA) of the wing relative to air flow [17]. The tunable impedance (TI) approach is one of the few methods developed for manipulation of wing pitch rotation [19]-[20]. It employs a mechanical structure at the wing base which allows for manipulation of mechanical impedance properties of the joint. These modifications can influence the pitch profile of wings without requiring changes in stroke profile [21]-[22]. Through adjusting the two impedance properties of stiffness and equilibrium point of the pitch joint, it is now possible to control lift and thrust more freely. Although TI is able to provide a higher degree of controllability compared to traditional wing-beat modification approaches [23], its lift and thrust manipulation procedures are not always completely decoupled [20].

In this work, we first identify the conditions that guarantee maximum decoupling between lift and thrust manipulation when TI approach is used. Under such conditions, sagittal motion of the vehicle is fully controllable. We then use these findings to develop a motion controller that is capable of tracking various trajectories in the sagittal plane with a considerably high degree of precision as verified by our simulated experiments.

The rest of the paper is organized as follows. Section II provides a brief review of the tunable impedance approach and how it is used for force manipulation. Decoupling conditions are then investigated in Section III. The MAV

H. Mahjoubi and K. Byl are with the Robotics Laboratory, Department of Electrical and Computer Engineering, University of California at Santa Barbara, Santa Barbara, CA 93106 USA (e-mail: h.mahjoubi@ece.ucsb.edu, katiebyl@ece.ucsb.edu).

model used in simulations and the designed motion controller are discussed in Section IV. Section V presents the results of several simulated trajectory tracking experiments. Finally, Section VI concludes the paper.

II. Tunable Impedance Approach: A Review

In [22], we argued that synchronous muscles may be insects' primary means for manipulation of wings' pitch profiles. It was shown that a joint and its clinging pair of muscles can be modeled as a torsional spring, i.e.:

$$\tau = k_{rot}\ (\psi - \psi_0) \qquad (1)$$

where τ is the torque produced due to rotation of the joint while k_{rot} and ψ_0 are the stiffness and equilibrium point of the spring, respectively. The wing pitch angle ψ is used as a measure of joint's rotation.

The torque in (1) should be in balance with the pitch torque produced by stroke motion of the wing, i.e.:

$$\tau = z_{CoP}\ F_N - b_\psi \dot{\psi} - J_\psi \ddot{\psi} \qquad (2)$$

in which, J_ψ and b_ψ are the moment of inertia and passive damping coefficient of the wing along its pitch rotation axis, respectively. F_N is the aerodynamic force component that is perpendicular to the surface of wing at its center of pressure (CoP). As illustrated in Fig. 1, z_{CoP} is the distance of CoP from wing's pitch rotation axis.

To find the pitch profile of a wing for any given set of impedance parameters, it is also necessary to have an approximation of aerodynamic forces in Fig. 1. The quasi-steady-state model described in [22] will be used to estimate these forces. The values of wing parameters used in all future simulations are reported in Table I. Note that for the chosen wing shape in Fig. 1, z_{CoP} is equal to 6.73% of the wing's span [20], i.e. R_W.

The tunable impedance approach suggests that by modification of impedance properties, one can manipulate pitch profile of either wing while its stroke profile remains

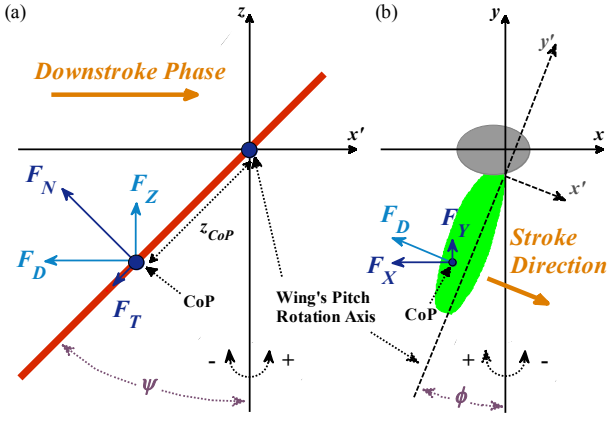

Fig. 1. (a) Wing cross-section (during downstroke) at center of pressure, illustrating the pitch angle ψ. Normal and tangential aerodynamic forces are represented by F_N and F_T. F_Z and F_D represent the lift and drag components of the overall force. (b) Overhead view of the wing/body setup which demonstrates the stroke angle ϕ. F_X and F_Y are components of F_D which represent forward and lateral thrust, respectively.

TABLE I
Physical Parameters Used in Simulations

Symbol	Description	Value
ρ	air density at sea level	1.28 kg/m^3
R_W	average span of each wing in a fly-sized flapping-wing MAV	1.5×10^{-2} m
J_ψ	moment of inertia of each wing (pitch rotation)	1×10^{-11} N.m.s^2
b_ψ	passive damping coefficient of each wing (pitch rotation)	5×10^{-10} N.m.s
m_{body}	estimated mass of a two-winged MAV with similar dimensions	7×10^{-5} kg
g	standard gravity at sea level	9.81 m/s^2

unperturbed – in this work $\phi = 50^\circ\sin(200\pi t)+\beta$ where the small and slowly variable bias angle β is the only applicable change to stroke profiles of both wings and has an insignificant effect on force production [22]. In fact, the value of k_{rot} primarily determines the range of variations in ψ (Fig. 2.a) which in turn affects the magnitude of aerodynamic forces (Fig. 2.b-c). Note that when $\psi_0 = 0^\circ$, pitch and thrust profiles are odd-symmetric, i.e. the average thrust is 0. Introducing a nonzero value of ψ_0 perturbs this symmetry (Fig. 2.f) by biasing the pitch profile (Fig. 2.d). In short, tunable impedance allows us to control overall lift and thrust by manipulating k_{rot} and ψ_0, respectively [22]. However, Fig. 2.c and 2.e suggest that each impedance parameter may also influence the other force.

III. Decoupled Lift/ Thrust Control: Conditions

To investigate the possibility of decoupled lift/thrust control via tunable impedance approach, we first need to model the relationships between impedance parameters and

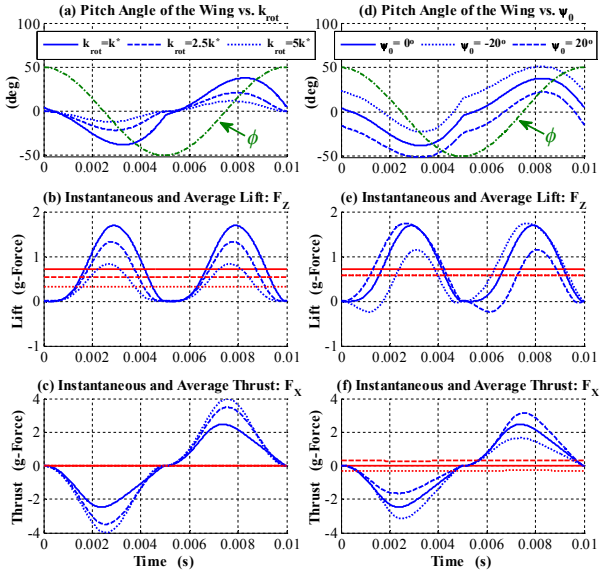

Fig. 2. (a) Pitch angle evolution of one wing for $\psi_0 = 0^\circ$ and different values of k_{rot} ($k^* = 2.7\times10^{-6}$ N.m/rad). The corresponding instantaneous (blue) and average (red) lift and forward thrust are plotted in (b) and (c), respectively. (d) Pitch angle evolution of one wing for $k_{rot} = k^*$ and different values of ψ_0. The corresponding instantaneous (blue) and average (red) lift and forward thrust are plotted in (e) and (f), respectively. All forces are normalized by the estimated weight of the vehicle.

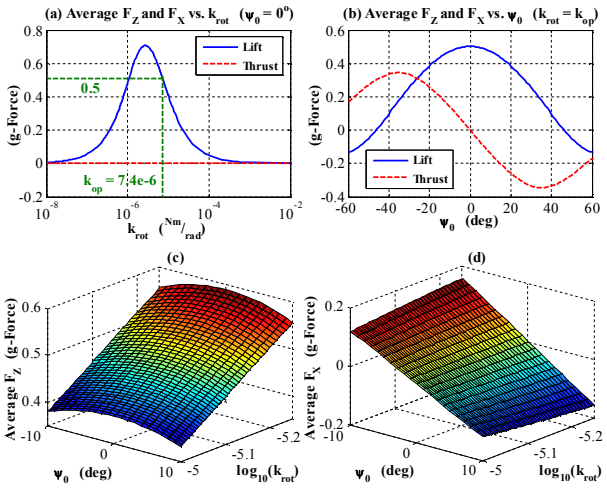

Fig. 3. (a) Average values of lift and thrust vs. k_{rot} when $\psi_0 = 0^\circ$. At $k_{rot} = k_{op} = 7.4\times10^{-6}$ N.m/rad, two wings will be able to produce sufficient lift for levitation. (b) Average values of lift and thrust vs. ψ_0 when $k_{rot} = k_{op}$. (c) Average lift for impedance values around $k_{rot} = k_{op}$ and $\psi_0 = 0^\circ$. (d) Average thrust for impedance values around $k_{rot} = k_{op}$ and $\psi_0 = 0^\circ$. All force values are normalized by the estimated weight of the vehicle.

these forces. We choose the average values of lift and thrust over intervals of 0.01 s – i.e. full stroke cycles – as our measure for influence of impedance parameters on aerodynamic forces.

Fig. 3.a illustrates the steady state values of these forces over a wide range of values for k_{rot} while ψ_0 is kept at 0°. It is easy to observe that for a MAV with two wings, $k_{rot} = k_{op} = 7.4\times10^{-6}$ N.m/rad and $\psi_0 = 0^\circ$ is an ideal operation point for hovering. In addition, it seems that in the vicinity of this point, average lift has an approximately linear relationship with $\log_{10}(k_{rot})$ (Fig. 3.c). Note that small values of ψ_0 have little influence on overall lift. Fig. 3.b illustrates the steady state values of these forces over a wide range of values for ψ_0 while k_{rot} is kept at k_{op}. When impedance values are close to $k_{rot}=k_{op}$ and $\psi_0=0^\circ$, a linear relationship between average thrust and ψ_0 is also observable (Fig. 3.d). Note that slight changes in k_{rot} from k_{op} have little influence on overall thrust.

The force values in Fig. 3 are calculated for constant impedance parameters. However, the linear relationships between steady-state values suggest that a linearized model around $k_{rot} = k_{op}$ and $\psi_0 = 0^\circ$ will be able to provide a reasonable approximation of dynamic behavior of these forces in response to varying impedance properties. To find this linear model, we employ system identification techniques – computation/smoothing of Empirical Transfer Function Estimates followed by subspace identification method [24] for transfer function matching – in order to identify components of the nonlinear MIMO system that relate impedance parameters to aerodynamic forces:

$$\Delta F_Z(s) = G_{ZK}(s)\ \Delta K(s) + G_{Z\Psi}\ \psi_0(s) \qquad (3)$$

$$\Delta F_X(s) = G_{XK}(s)\ \Delta K(s) + G_{X\Psi}\ \psi_0(s) \qquad (4)$$

ΔF_Z and ΔF_X represent the changes in lift and forward thrust due to modifications in k_{rot} and ψ_0. Note that $\Delta K = \log_{10}(k_{rot} / k_{op})$. Each G represents a transfer function from an impedance parameter to a force component as indicated by its subscripts. In all system identification experiments, limits of $|\Delta K| < 0.05$ and $|\psi_0| < 0.1$ rad were applied.

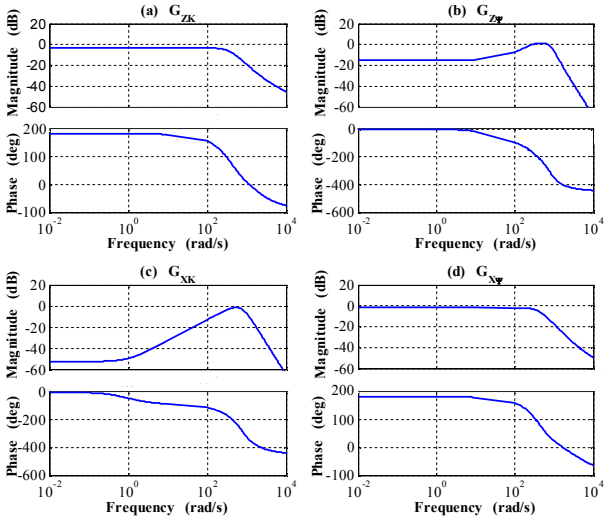

Fig. 4. The Bode diagrams of identified subsystems from impedance parameters to average aerodynamic forces: (a) G_{ZK}, (b) $G_{Z\Psi}$, (c) G_{XK}, (d) $G_{X\Psi}$.

The Bode diagrams of identified subsystems are plotted in Fig. 4. In low frequencies, both G_{ZK} and $G_{X\Psi}$ have steady-state gains close to 0 dB, while in comparison, the same gains for $G_{Z\Psi}$ and G_{XK} are well below unity. Therefore, we expect that respective disturbances due to stiffness/ equilibrium point manipulation on thrust/lift control will be insignificant in the low frequency range, allowing decoupled control of these forces.

To choose a suitable upper limit for this range, we use the evaluation parameters that are illustrated in Fig. 5. To calculate these values, three groups of numerical experiments have been performed. In the first group, sinusoidal waves of magnitude 0.05 and different frequencies were used for ΔK while $\psi_0 = 0$ rad. Lift and

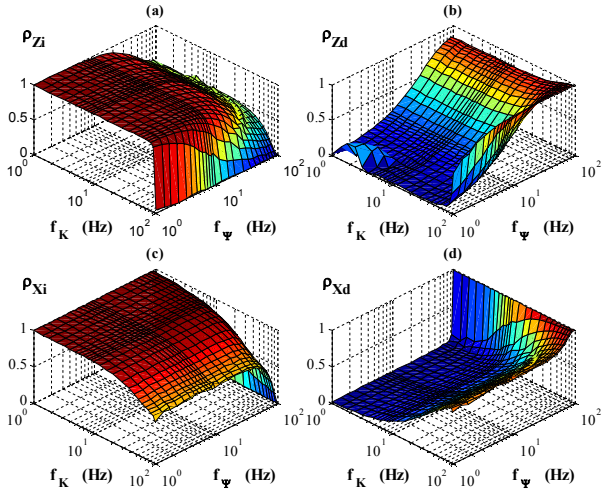

Fig. 5. Correlation coefficient vs. frequency of mechanical impedance manipulation for (a) desired and overall lift, (b) disturbance and overall lift, (c) desired and overall thrust, (d) disturbance and overall thrust.

thrust outputs in this case are treated as desired and disturbance, respectively. In the second group, sinusoidal waves of magnitude 0.1 rad and different frequencies were used for ψ_0 while $k_{rot} = k_{op}$. Lift and thrust outputs in this case are treated as disturbance and desired, respectively. Finally, the third group of experiments uses both described nonzero inputs at the same time. Lift and thrust outputs in this case are the overall results of impedance manipulation. Correlation values between desired (disturbance) and overall lift are plotted in Fig. 5.a (5.b). Correspondingly, correlation values between desired (disturbance) and overall thrust are plotted in Fig. 5.c (5.d).

From Fig. 5, when the frequency content of both inputs is below 10 Hz, the correlation between desired and overall values of either force is above 0.97 while the correlation between disturbance and overall values remains below 0.31. Thus, by removing the frequency content of ΔK and ψ_0 above 10 Hz, decoupling of lift/thrust control will be significantly improved.

IV. MAV Model and Flight Control

Based on the observations in Section III, a simple motion controller is developed to track reference trajectories in the sagittal plane. Simulated experiments in Section V employ this controller along with a six DoF model of the MAV. A brief review of this model and the designed controller are presented next.

A. Dynamic Model of the MAV

The free-body diagram of a typical two-winged flapping-wing MAV [7] is shown in Fig. 6. The six DoF dynamic model [17] of the vehicle is developed by applying Newton's equations of motion in this body frame. Related details are available in [22]. Employed values for model parameters are reported in Table II.

B. Motion Controller

Fig. 7 illustrates the block diagram of the designed motion controller. Pitch angle of the body, i.e. θ_{pitch}, is stabilized at 0 rad through smooth biasing ($|\beta| \leq 0.26$ rad) of the stroke

TABLE II
Characteristics of the Modeled Flapping-Wing MAV

Symbol	Description	Value
b_ω	passive damping coefficient of the body (rotation)	3×10^{-6} N.m.s
b_v	viscous friction coefficient of the body when moving in the air	1×10^{-4} N.s^2/m^2
J_{body}	inertia matrix of the body relative to CoM	$3I_{3\times3}\times10^{-8}$ N.m.s^2
$H(\psi=0^\circ)$	distance of CoP from transverse plane of the body (xy in Fig. 6) when $\psi=0^\circ$	4.4×10^{-3} m
$R(\phi=0^\circ)$	distance of CoP from sagittal plane of the body (xz in Fig. 6) when $\phi=0^\circ$	1.19×10^{-2} m
$U(\phi=0^\circ)$	distance of CoP from coronal plane of the body (yz in Fig. 6) when $\phi=0^\circ$	1.08×10^{-4} m
W_{body}	body width at the base of wings	2.16×10^{-3} m

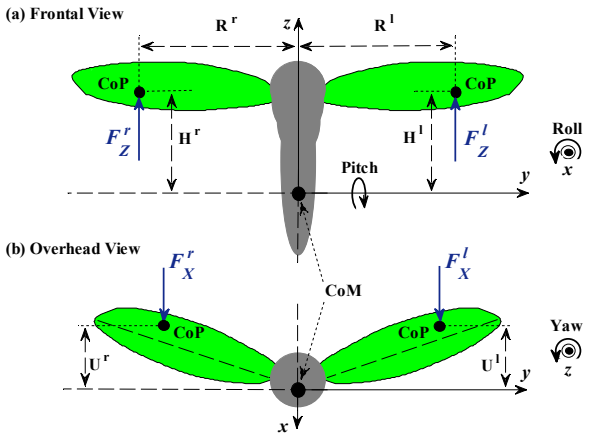

Fig. 6. Free-body diagram model of a flapping-wing MAV: (a) frontal and (b) overhead views. H, R and U are the distance components of center of pressure (CoP) of each wing from center of mass (CoM) of the model. For simulation purposes, Euler angles in Tait-Bryan ZXY convention are employed to update the orientation of the body.

angle [22]. A PD sub-controller, $10+0.05s/(10^{-3}s+1)$, is used for this purpose. The observer block in Fig. 7 applies the force approximations in (3) and (4) along with (5) and (6) to estimate velocity of the model along Z and X axes:

$$m_{body}\,\dot{\hat{Z}}_d = 2\Delta F_Z - b_v\,\hat{Z}_d\left|\hat{Z}_d\right| \quad (5)$$

$$m_{body}\,\dot{\hat{X}}_d = 2\Delta F_X - b_v\,\hat{X}_d\left|\hat{X}_d\right| \quad (6)$$

where $\hat{Z}_d$ and $\hat{X}_d$ represent these estimations, respectively. Mass of the model is shown by m_{body} (Table I) and b_v is the viscous friction coefficient (Table II). Actual displacements and approximated velocities are used by manually tuned proportional lift (gain: [100 5]) and thrust (gain: [2000 100]) sub-controllers to manipulate impedance properties of the wings – ΔK and ψ_0 are limited to [-0.4 0.26] and [-0.35 rad 0.35rad], respectively. Note that both wings always have the same values of β, k_{rot} and ψ_0, resulting in ideally 0 lateral thrust and roll/yaw torques due to symmetry. Thus, we assume that position of the body along Y axis and its roll/yaw angles remain 0 throughout all experiments. Simulations are then effectively restricted to motion in the sagittal plane (XZ).

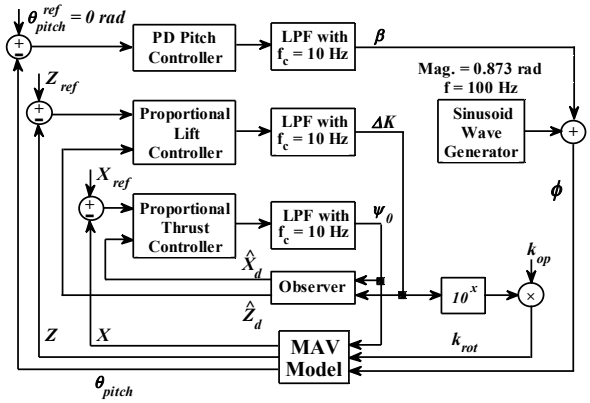

Fig. 7. Block diagram of the proposed motion controller in interaction with MAV model. Cutoff frequency f_c of each employed filter is set to 10 Hz. Both wings use the same values of β, k_{rot} and ψ_0 at all times.

V. Simulated Experiments

Motion of the model along various trajectories in the *XZ* plane has been simulated. In every experiment, the model is initially hovering at $X = 0$ m and $Z = 0$ m, i.e. $X_{ref} = 0$ m and $Z_{ref} = 0$ m. Later, new reference position profiles are introduced to sub-controllers that guarantee a smooth velocity profile over desired trajectory. We observed that as long as acceleration demands of these profiles are within the capabilities of the model – primarily due to enforced limits on ΔK and ψ_0 – tracking will be achieved with a considerably high degree of precision. The results of simulated experiments with three important types of trajectories are presented next.

A. Strictly Horizontal (Vertical) Maneuvers

As the most trivial group of maneuvers, the vehicle must be able to maintain its position on one axis while moving along the other one. Fig. 8 demonstrates the results of tracking a square trajectory that requires all of these maneuvers, i.e. takeoff, landing and forward/backward motion. As it can be seen, the controller successfully handles such maneuvers and keeps close to the reference trajectory (Fig. 8.g).

B. Simultaneous Displacements: A Linear Trajectory

To investigate the effectiveness of our approach to decoupled lift/thrust control, different trajectories with displacements along both *X* and *Z* axes were examined. A simple example of such trajectories is a straight line with a slope of -1. Simulation results for the corresponding experiment are illustrated in Fig. 9. A combination of backward flight and takeoff motion starting at t = 1 s enables the vehicle to reach $X = -0.5$ m and $Z = 0.5$ m by t = 2 s. At this point, the direction of motion is reversed. Through simultaneous descent and forward flight, the vehicle returns to its original position at t = 3 s. All the while, the slope of its trajectory remains close to -1 (Fig. 9.g).

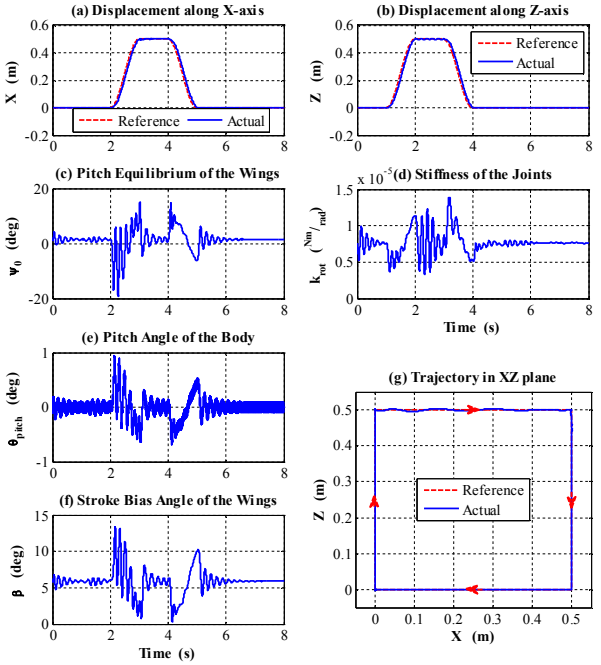

Fig. 8. Results for tracking a square trajectory: displacement along (a) *X* and (b) *Z* axes, (c) pitch equilibrium of the wings ψ_0, (d) stiffness of the joints k_{rot}, (e) pitch angle of the body θ_{pitch}, (f) stroke bias angle of the wings β and (g) overall trajectory in *XZ* plane.

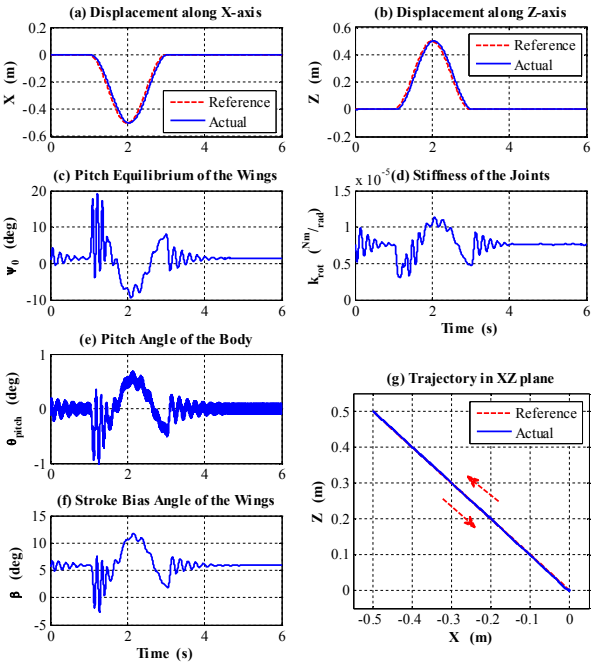

Fig. 9. Results for tracking a linear trajectory with a slope of -1: displacement along (a) *X* and (b) *Z* axes, (c) pitch equilibrium of the wings ψ_0, (d) stiffness of the joints k_{rot}, (e) pitch angle of the body θ_{pitch}, (f) stroke bias angle of the wings β and (g) overall trajectory in *XZ* plane.

C. Motion along Curves

Curves are a more complex case of trajectories with simultaneous displacement along both *X* and *Z* axes. The results of an experiment with a partially circular reference trajectory are plotted in Fig. 10. The controller still manages to follow this trajectory with high precision (Fig. 10.g). Note that compared to other trajectories, correction of motion over curves requires smaller changes in impedance parameters (Fig. 10.c and d). This is partially due to the fact that stable motion along such trajectories is rarely accompanied by high velocities and/or acceleration rates.

VI. Conclusion

Inspired by insect flight, tunable impedance has been previously proposed as a semi-passive method for force manipulation in flapping-wing MAVs. This approach states that pitch rotation profile of each wing can be modified through changes in mechanical impedance properties of its joint. Consequently, magnitude of variations and average value of this profile are influential factors in regulation of aerodynamic forces (Fig. 2).

The main advantage of TI over common methods of force control is its ability to operate with a fixed stroke profile.

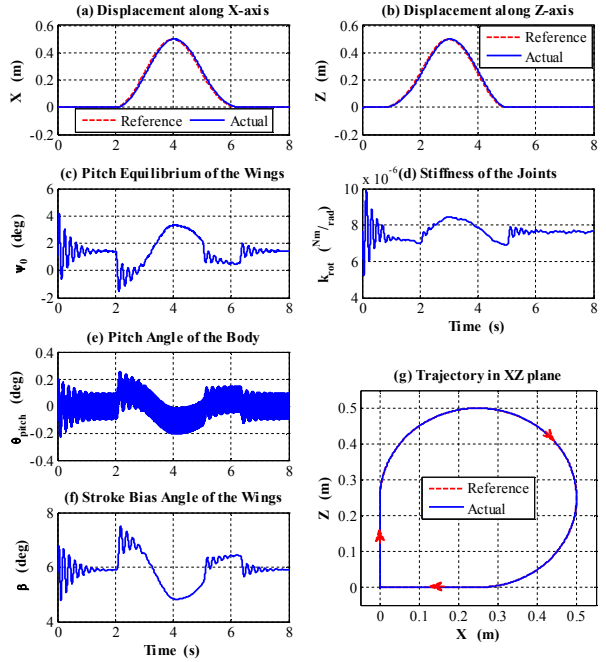

Fig. 10. Results for tracking a partially circular trajectory: displacement along (a) X and (b) Z axes, (c) pitch equilibrium of the wings ψ_0, (d) stiffness of the joints k_{rot}, (e) pitch angle of the body θ_{pitch}, (f) stroke bias angle of the wings β and (g) overall trajectory in XZ plane.

This effectively simplifies the control system and can reduce the amount of onboard hardware in an actual prototype. Under this approach, the system is also more controllable and has a higher degree of mobility [23]. However, lift and thrust control are not completely decoupled which at times may result in limited maneuverability of the vehicle.

In this work, we showed that in a system with TI as its underlying strategy for force control, coupling between lift and thrust effectively occurs when either impedance variable carries significant components at frequencies close to the wing-beat rate (Fig. 5). Removing high frequency content from both impedance values will considerably improve decoupling between lift and thrust and results in better performance compared to our previous work [23]. In fact, a simple control structure such as Fig. 7 is sufficient to stabilize motion along given trajectories. Results of simulated experiments verify the tracking capabilities of this method.

It was observed that as long as a trajectory can be defined by smooth velocity profiles, the only concern for successful tracking is the corresponding acceleration requirements. While imposed limits on impedance parameters guarantee linear relationships with forces, they also restrict acceleration capabilities of the model (Fig. 3). Thus, successful tracking also requires that time-derivatives of these velocity profiles lie within acceleration limits of the model. In a real system, designing such profiles relies on information from both environment and vehicle itself. A high level controller must first come up with an appropriate trajectory based on surroundings of the vehicle and relative location of its target. The current velocity and acceleration limits of the MAV must then be treated as constraints of designing a suitable velocity profile for tracking purposes.

REFERENCES

[1] M. F. M. Osborne, "Aerodynamics of flapping flight with application to insects," *J. Exp. Biol.*, 28(2), pp. 221-245, 1951.

[2] C. P. Ellington, "The aerodynamics of hovering insect flight I. the quasi-steady analysis," *Philos. Trans. R. Soc. Lond. B. Biol. Sci.*, 305(1122), pp. 1-15, 1984.

[3] M. H. Dickinson, F. Lehmann, and S. P. Sane, "Wing rotation and the aerodynamic basis of insect flight," *Science*, 284 (5422), pp. 1954-1960, 1999.

[4] D. Floreano, J. C. Zufferey, M. V. Srinivasa, and C. P. Ellington, Flying Insects and Robots, Springer, 2009.

[5] B. Cheng, and X. Deng, "Near-hover dynamics and altitude stabilization of an insect model," in Proc. American Control Conf. (ACC), pp. 39-44, June 30-July 2, 2010.

[6] S. P. Sane, "Steady or unsteady? uncovering the aerodynamic mechanisms of insect flight," *J. Exp. Biol.*, 214, pp. 349-351, 2011.

[7] R. J. Wood, "The first takeoff of a biologically inspired at-scale robotic insect," *IEEE Trans. on Robot.*, 24, pp. 341–347, 2008.

[8] G. De Croon, K. De Clerq, R. Ruijsink, B. Remes, C. De Wagter, "Design, aerodynamics, and vision-based control of the DelFly," *Int. J. MAV*, 1 (2), pp. 71-97, 2009.

[9] V. Arabagi, "Design and manufacturing of a controllable miniature wing robotic platform," *Int. J. Robot. Research*, 31(6), pp. 785-800, 2012.

[10] F. Y. Hsiao, C. L. Chen, and J. F. Shen, "Altitude control of flapping-wing MAV using vision-base navigation," in Proc. American Control Conf. (ACC), pp. 21-26, June 30-July 2, 2010.

[11] N. O. Perez-Arancibia, G. L. Barrows, and R. J. Wood, "Altitude feedback control of a flapping-wing microrobot using an on-board biologically inspired optical flow sensor," in Proc. IEEE Int. Conf. Robotics and Automation (ICRA), pp. 4228-4235, May 14-18, 2012.

[12] R. Malhan, M. Benedict, and I. Chopra, "Experimental studies to understand the hover and forward flight performance of a MAV-scale flapping wing concept," *J. American Helicopter Soc.*, 57, pp. 1-11, 2012.

[13] D. B. Doman, M. W. Oppenheimer, and D. O. Sigthorsson, "Wingbeat shape modulation for flapping-wing micro-air-vehicle control during hover," *J. Guidance Control and Dynamics*, 33(3), pp. 724-739, 2010.

[14] E. Jones, and G. Vachtsevanos, "Fixed frequency, variable amplitude (FiFVA) actuation systems for micro aerial vehicles," in Proc. IEEE Int. Conf. Robotics and Automation (ICRA), pp. 165-171, May 9-13, 2011.

[15] N. O. Perez-Arancibia, J. P. Whitney, and R. J. Wood, "Lift force control of flapping-wing microrobots using adaptive feedforward schemes," *IEEE Trans. Mechatronics*, 18(1), pp. 155-168, 2013.

[16] D. B. Doman, and M. W. Oppenheimer, "Dynamics and control of a minimally actuated biomimetic vehicle: part II. control," AIAA Guidance, Navigation, and Control Conf., August 10-13, 2009.

[17] X. Deng, L. Schenato, W. C. Wu, and S. S. Sastry, "Flapping flight for biomimetic robotic insects: part I–system modeling," *IEEE Trans. Robot.*, 22(4), pp. 776–788, 2006.

[18] A. J. Bergou, S. Xu and Z. J. Wang, "Passive wing pitch reversal in insect flight," J. Fluid Mech., 591, pp. 321–337, 2007.

[19] H. Mahjoubi, and K. Byl, "Analysis of a tunable impedance method for practical control of insect-inspired flapping-wing MAVs," In Proc. IEEE Conf. on Decision and Control and European Control Conf. (CDC-ECC), pp. 3539-3546, December 12-15, 2011.

[20] H. Mahjoubi, and K. Byl, "Tunable impedance: a semi-passive approach to practical motion control of insect-inspired MAVs," in Proc. IEEE Int. Conf. Robotics and Autom. (ICRA), pp. 4621-4628, May 14-18, 2012.

[21] H. Mahjoubi, and K. Byl, "Insect flight muscles: inspirations for motion control in flapping-wing MAVs," in Proc. Int. Conf. Unmanned Aircraft Systems (ICUAS), June 12-15, 2012.

[22] H. Mahjoubi, and K. Byl, "Modeling synchronous muscle function in insect flight: a bio-inspired approach to force control in flapping-wing MAVs," *J. Int. & Robotic Systems*, 70 (1-4), pp. 181-202, 2013. (Available Online, DOI: http://dx.doi.org/10.1007/s10846-012-9746-x)

[23] H. Mahjoubi, and K. Byl, "Steering and horizontal motion control in insect-inspired flapping-wing MAVs: the tunable impedance approach," in Proc. American Control Conf. (ACC), pp. 901-908, June 27-29, 2012.

[24] T. McKelvey, H. Akcay, and L. Ljung, "Subspace-based multivariable system identification from frequency response data," *IEEE Trans. Automatic Control*, 41(7), pp. 960-979, 1996.